Localization of Epileptogenic Zones in F-18 FDG Brain PET of Patients with Temporal Lobe Epilepsy Using Artificial Neural Network

Jae Sung Lee, *Student Member, IEEE*, Dong Soo Lee*, *Member, IEEE*, Seok-Ki Kim, Sang-Kun Lee, June-Key Chung, Myung Chul Lee, and Kwang Suk Park, *Member, IEEE*

***Abstract*—For an objective interpretation of cerebral metabolic pattern to find epileptogenic zones in patients with temporal lobe epilepsy (TLE), we developed a computer-aided classifier using an artificial neural network (ANN). We studied 261 epilepsy patients diagnosed as no abnormal findings (NA, $n = 64$), left TLE ($n = 116$), or right TLE ($n = 81$) on interictal brain F-18-flurodeoxyglucose positron emission tomography (FDG PET) by the consensus of two expert physicians. Seventeen asymmetry indexes between the mean counts of the 34 mirrored regions were extracted from the spatially normalized images and used as input parameters. The three diagnoses of NA, left TLE, and right TLE were used as outputs of the ANN. The structure of the ANN was optimized with variable error goals and the number of hidden units. On the criteria of agreement of diagnoses with those of expert viewers, the best classifier was chosen, which yielded a maximum average agreement of 85% for the test set when we used an error goal of 20 (sum of squared error) and ten hidden units. We could devise an ANN that performed as well in diagnosing left or right TLE on FDG PET as human experts and could be used as a clinical decision support tool.**

***Index Terms*—Artificial neural network, brain PET, epilepsy, spatial normalization.**

I. Introduction

LOCALIZATION of epileptogenic zones is the most important step in selecting patients with medically intractable focal epilepsy for potential surgical cures. The locations of epileptogenic zones are found using the clinical criteria produced by the sum of noninvasively acquired findings, such as clinical semiology, ictal and interictal electroencephalogram (EEG), magnetic resonance image (MRI), F-18-flurodeoxyglucose positron emission tomography (FDG PET), and ictal and interictal perfusion single photon emission computed tomography (SPECT) [1]–[3].

Manuscript received March 14, 1999; revised February 14, 2000. This work was supported in part by the Research Fund of the Ministry of Science and Technology of Korea and in part by BK21 Human Life Sciences. The Associate Editor responsible for coordinating the review of this paper and recommending its publication was C. J. Thompson. *Asterisk indicates corresponding author.*

J. S. Lee is with the Interdisciplinary Program in Medical and Biological Engineering Major, Seoul National University, Seoul, Korea.

*D. S. Lee, S.-K. Kim, J.-K. Chung, and M. C. Lee are with the Department of Nuclear Medicine, College of Medicine, Seoul National University, Seoul 110-799, Korea (e-mail: dsl@palza.snu.ac.k).

S.-K. Lee is with the Department of Neurology, College of Medicine, Seoul National University, Seoul 110-799, Korea.

K. S. Park is with the Department of Biomedical Engineering, College of Medicine, Seoul National University, Seoul 110-799, Korea.

Publisher Item Identifier S 0278-0062(00)04504-3.

Epileptogenic zones show characteristic decreased glucose metabolism on FDG PET. The diagnostic accuracy of FDG PET has been found to be 70–85% according to cumulated analyses of reports in the literature [1], [3]. FDG PET has been found to be extremely helpful for localization of epileptogenic zones, especially in patients without prominent structural abnormality. However, hypometabolic regions on FDG PET were not confined to epileptogenic zones. Adjacent or even remote cortical areas beyond epileptogenic zones could show decreased glucose metabolism. Experienced nuclear medicine physicians have been trained to recognize exact epileptogenic zones by analyzing metabolic patterns referring to the final surgical outcome and the combined information obtained from clinical semiology, MRI, ictal EEG and ictal SPECT. They apply these criteria to their interpretation of PET images to localize epileptogenic zones.

Artificial neural networks (ANN's) had recently been applied to an automated interpretation of functional brain images. These were used for differentiating Alzheimer's disease or vascular dementia from normal aging on FDG PET or perfusion SPECT [4]–[10]. In these studies, multiple regions of interest (ROI's) had been drawn manually to find out the characteristic distribution pattern of cerebral metabolism or perfusion [4]–[10]. The manual drawing of ROI's on individual images was so time consuming and subjective that the development of automatic spatial normalization was mandatory and a prerequisite for the development of an automatic interpretation system.

In this study, an artificial intelligence system was designed for interpreting FDG PET to find epileptogenic zones based on the diagnostic criteria and the decision rules of human experts. We adopted a spatial normalization method [11]–[16] using a standardized template of PET images. Asymmetric indexes of mirrored regions to the midline were used for 17 cerebral regions from predefined volumes of interest (VOI's) on the template. Using these asymmetry indexes as input parameters and the correct diagnoses as output nodes, characteristic features were extracted using the scheme shown in Fig. 1 and the agreement rates were enhanced and optimized by varying error goals and hidden nodes.

The performance of optimized ANN was compared to those of linear discriminant analysis and another human expert who was not involved in the gold standard classification, in order to judge whether the performance of ANN is superior to a more traditional technique and is clinically acceptable or not.

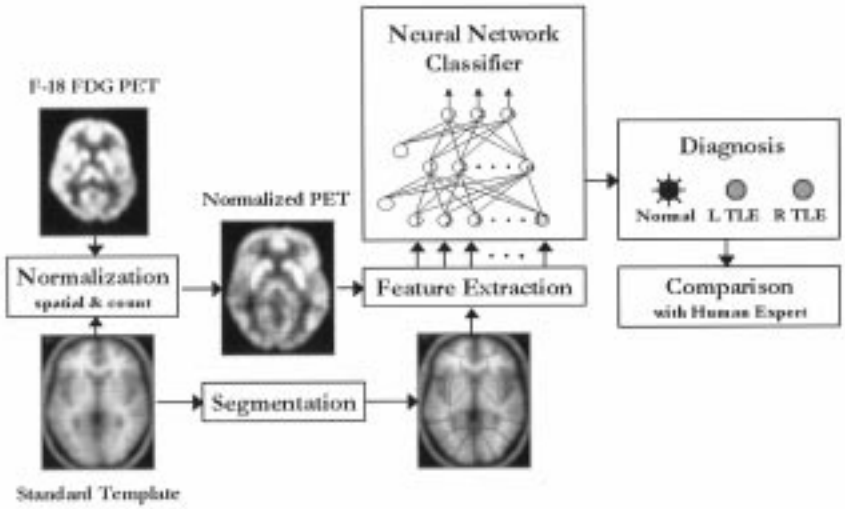

Fig. 1. Schematic diagram of the automatic interpretation system for epileptogenic zones on FDG PET.

II. Methods

A. Patient Population

Three hundred and twenty-five epilepsy patients who underwent brain FDG-PET were classified by the diagnosis made with visual interpretation by two experienced nuclear physicians. Pediatric patients less than 15 years old and patients with gross structural abnormalities on MRI were excluded. To meet the need for a sufficient amount of data for the training of the ANN, patient groups with small numbers of patients were excluded. Patients with no abnormal findings (NA, $n = 64$), left temporal lobe epilepsy (TLE) (left TLE, $n = 116$) or right temporal lobe epilepsy (right TLE, $n = 81$) were selected for inclusion in this study. There were 261 patients ($\text{male} : \text{female} = 160 : 101, 29.6 \pm 8.8$ years old) in all. Seventy of these patients underwent surgery and were followed for more than six months. Fifty-two of the 53 surgically treated TLE patients showed favorable outcomes (Engel class I or II) and were confirmed to have left TLE or right TLE. Seventeen of the subjects with normal FDG PET were operated on after invasive study. Thirteen showed favorable outcomes (Engel class I or II), and were confirmed to have neocortical or temporal lobe epilepsy.

B. PET

370 MBq (10 mCi) of F-18-FDG was injected, and PET studies were performed on an ECAT EXACT 47 scanner (Siemens-CTI, Knoxville, TN). Transaxial images were reconstructed with a Shepp filter (cutoff $= 0.30$ cycles/pixel) as 128 $\times$ 128$\times$ 47 matrices with a size of 2.1 $\times$ 2.1 $\times$ 3.4 mm.

C. Image Analysis and Feature Extraction

All the PET images were converted to the ANALYZE format (The Mayo Clinic, Rochester, NY) and were transferred to the SPM96 program (Statistical Parametric Mapping 96, Institute of Neurology, University College of London, U.K.) for spatial normalization.

Header files and image matrices comprising transverse slices running from the bottom to the top of the brain were separated and reformatted. Image files in ANALYZE format were spatially normalized into the MNI (Montreal Neurological Institute, McGill University, Montreal, Canada) standard template using the SPM96 [12], [13]. Affine transformation was performed to determine the 12 optimal parameters to register the brain on the template. Subtle differences between the transformed image and the template were removed by the nonlinear registration method using the weighted sum of the predefined smooth basis functions used in discrete cosine transformation. Spatially normalized images were smoothed by convolution with an isotropic Gaussian kernel with 16 mm full width at half maximum (FWHM) to suppress noise or residual differences in the gyral anatomy. The count of each voxel was normalized to the whole count of cortical areas to compensate for the difference in global count caused by the amount of the total injected dose and individual uptake characteristics.

After these spatial and count normalizations, the features representing the pattern of cerebral metabolism were extracted from the predefined volumes of interest (VOI) on the standard template. Seventeen asymmetry indexes of mirrored regions to the hemispheric midline were calculated from 34 VOI's of cerebral regions on the standard template and spatially normalized images. Table I shows these 17 cerebral regions on each hemisphere and their abbreviations. Since the most relevant characteristic abnormal findings on FDG PET in the patients with TLE was an asymmetrically decreased metabolism of temporal and adjacent lobes, the largest asymmetry was closely related to the location of epileptogenic zones. The asymmetry index of the mirrored regions was defined as the following equation and used for the input parameter:

$$\text{AI} = \frac{C_r - Cl}{C_r + C_l}$$

C_r and C_l are the mean counts of the regions (VOI's) in the right and left hemispheres, respectively.

D. Neural Network Classifier

An ANN classifier was designed in the environment of Matlab 5.1 (Mathworks, Natick, MA) to automatically interpret the cerebral metabolic patterns of epilepsy patients. A

TABLE I
BRAIN AREAS AND THEIR ABBREVIATIONS DEFINED FOR THE SEGMENTATION OF THE STANDARD TEMPLATE: THE BRAIN WAS SEGMENTED INTO 34 AREAS (17 AREAS IN EACH HEMISPHERE) CONVENTIONALLY USED IN THE INTERPRETATION OF FDG PET IMAGES BY EXPERIENCED NUCLEAR PHYSICIANS

Brain regions	Abbreviations
Superior Frontal	SF
Inferior Frontal	IF
Anterior Frontal	AF
Posterior Frontal	PF
Central Frontal	CF
Anterior Temporal	AT
Posterior Temporal	PT
Medial Temporal	MT
Lateral Temporal	LT
Superior Temporal	ST
Superior Parietal	SP
Inferior Parietal	IP
Primary Visual	PV
Associative Visual	AV
Cerebellum	CE
Basal Ganglia	BG
Thalamus	TH

three-layer feedforward error backpropagation neural network with 17 input nodes and three output nodes was used [17], [18]. The structure of our network is shown in Fig. 2. This network was trained to interpret metabolic patterns and produce identical diagnoses to those of expert viewers. The asymmetry indexes of the mirrored regions were normalized to have the same mean and standard deviations $(\text{mean} = 0, \text{standard deviation} = 1)$. These 17 indexes were provided for each input node as the summarized information of PET images for our neural network. Output nodes were set to $[1\ 0\ 0]^T$ for NA, $[0\ 1\ 0]^T$ for left TLE, and $[0\ 0\ 1]^T$ for right TLE. Sigmoid function was selected as the activation function of each node and gave the diagnostic output value in the range of $[0\ 1]$. Momentum and an adaptive learning rate were used to improve the performance of the network and accelerate its learning speed. Initial weights and biases were distributed randomly. The number of training epochs was constrained to 600.

E. Optimization and Performance Evaluation of the ANN

To find the optimal structure of the ANN, it was tested with variable error goals as the criteria to stop the training.

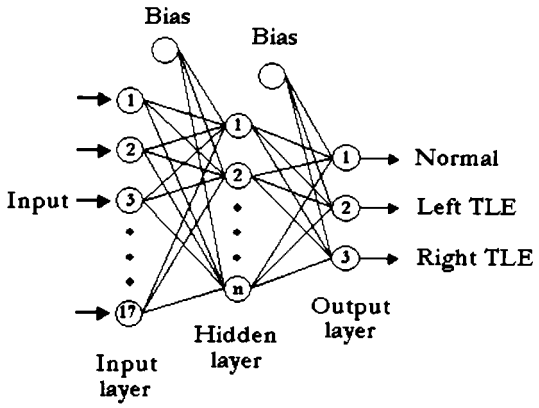

Fig. 2. Structure of a three-layer neural network: one hidden layer, 17 input nodes, and three output nodes.

The number of nodes in the hidden layer (hidden units) was also varied. The error signal at the jth output neuron at the presentation of the nth training pattern was defined by

$$e_j(n) = d_j(n) - y_j(n)$$

where $d_j(n)$ is the desired response for neuron j at pattern n and $y_j(n)$ is the output signal appearing at it.

The sum of squared error was obtained by summing the squared error over all j and n, as shown by

$$E = \sum_{n=1}^{N} \sum_{j=1}^{3} e_j^2(n)$$

where N denote the total number of patterns contained in the training set.

The ANN's were designed to stop the training when the sum of squared error reached their error goals. Error goals were set in the range of 5–50 in increments of five. The number of hidden units was set in the range of 5–30 in increments of five. The ANN was trained using 40 randomly selected images from each group. The performance of each ANN was tested using the remaining 141 images (NA 24, left TLE 76, and right TLE 41) (Table II).

The training and test sets were selected from the whole subject population in a random fashion 100 times. With each randomized test, ANN's were composed with variable error goals and numbers of hidden units. For each ANN, 50 experiments were performed with a randomized initial condition for weights and biases, and their performances (agreement rates of the diagnoses of ANN's with those of human experts) were averaged. A resulting performance map displaying the average agreement ratio for the pairs of error goals and the number of hidden units was composed. Finally, the performance maps from the 100 randomized training and test sets were averaged. In this way, the final optimal structure of the ANN classifier was selected. The schema of this procedure is summarized in Fig. 3. The performance of the final optimal ANN was analyzed for concordant and discordant cases.

TABLE II
NUMBER OF SUBJECTS FOR NEURAL NETWORK CLASSIFICATION

Diagnosis	Training set	Test set	Total
No abnormal findings (NA)	40	24	64
Left temporal lobe epilepsy (L TLE)	40	76	116
Right temporal lobe epilepsy (R TLE)	40	41	81

```
for (from 1 to 100)
  Random casting of training set
  for (from 5 to 100 with increment of 5)          % number of hidden units
    for (from 5 to 50 with increment of 5)         % error goal
          for (from 1 to 50)
            1. Random generation of initial weight and bias
            2. Training of neural network
            3. Test of trained network
      end
      Averaging of the agreement rates from 50 experiments
    end
  end
end
Averaging of the 100 randomized tests
```

Fig. 3. Procedure of the experiment to find the optimal structure of the ANN.

F. Comparison to Other Methods

To compare the performance of ANN against a more traditional statistical technique, linear discriminant analysis was performed on the same 100 training and test sets, which is implemented in the statistical toolbox of Matlab.

To judge whether the performance of ANN is clinically acceptable or not, an expert other than those involved in the gold standard classification performed blind classification and the result was compared with that of ANN. Since he had been trained for four years by the experts who had classified the PET images in the first place, he was appropriate for the comparison with ANN. He was blind to individual clinical diagnoses, examined each PET scan, and assigned one of the three diagnoses.

III. RESULTS

A. Feature Extraction

Spatial normalization was performed successfully on all the PET images. Profiles of the mean asymmetry indexes of the mirrored regions in NA (circle and solid line), left TLE (triangle and solid line), and right TLE (square and solid line) groups are shown in Fig. 4. Positive and negative values for asymmetry indexes indicated hypometabolism at left and right cerebral hemispheres, respectively. Asymmetry indexes in the NA group did not deviate from value zero and lay within the range of $\pm 1\%$. The asymmetry indexes of the left TLE and right TLE groups showed asymmetry in the respective hemispheres and these indexes were more prominent in the temporal lobes (AT, PT, MT, LT, and ST).

B. Optimization and Performance Evaluation of the ANN

An averaged performance map is displayed according to the error goals and the number of hidden units in Fig. 5. The performance of the network could be optimized at the error goal of 20 (sum of squared error). The number of hidden units did not seem to significantly influence the performance of the networks. However, the agreement rate tended to increase as the number of hidden units decreased. The agreement rate was maximal with ten hidden units. The network showed a maximum average agreement rate when it was trained with ten hidden units and an error goal of 20. The maximum average agreement rate was 85.0%.

C. Analysis of the Performance of the Optimized Network

The performance of ANN with optimized structure (ten hidden units and an error goal of 20) was superior to those of linear discriminant analysis and blind classification by the other human expert (Table III). Comparison data of the diagnoses by each method and the gold standard is summarized in Tables IV–VI. Data of ANN and linear discriminant analysis were the results for the test sets. All three had agreement rates of more than 80% for both the TLE groups, however, linear discriminant analysis and the other expert had lower performance for the discrimination of the NA group from the TLE groups (14.1% and 57.8%, respectively). Rarely did ANN, moreover, indicate contralateral hemispheres for the TLE group (1.5% for left TLE and 0.5% for right TLE). This high lateralization accuracy was comparable or superior to the expert (1.7% for left TLE and 3.7% for right TLE). Linear discriminant analysis showed the lowest performance in this characteristic as well (16.5% for left TLE and 14.5% for right TLE).

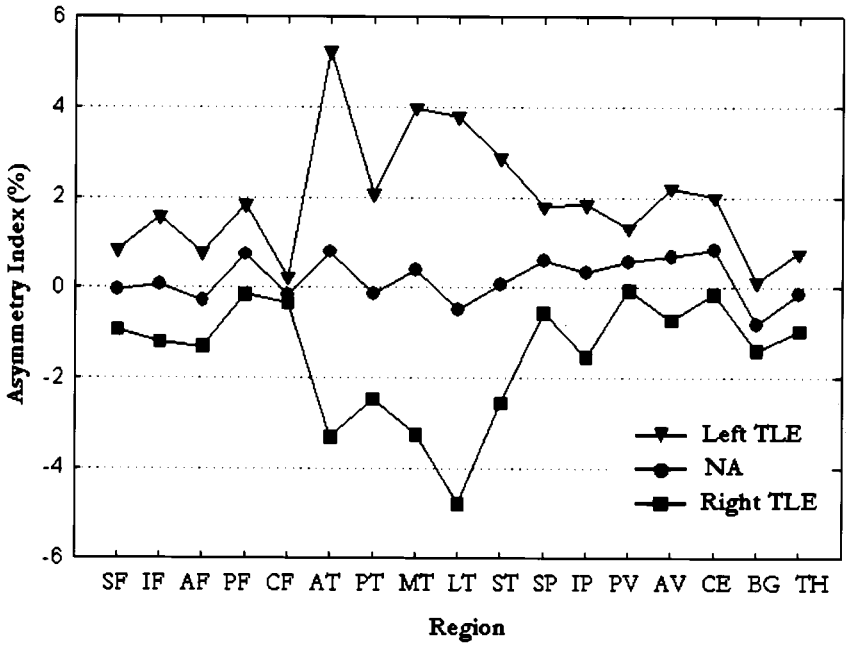

Fig. 4. Profile of the asymmetry indexes of mirrored regions in NA (circle and solid line), left TLE (triangle and solid line), and right TLE (square and solid line) groups. Profile of NA group did not diverse from the $y = 0$ line. Those of left TLE and right TLE groups showed the obvious deviation represented by asymmetric metabolism. In particular, the asymmetry of temporal areas (AT, PT, MT, LT, and ST) was more apparent than any other areas. x axis: 17 brain areas, y axis: mean asymmetry index between right and left hemisphere.

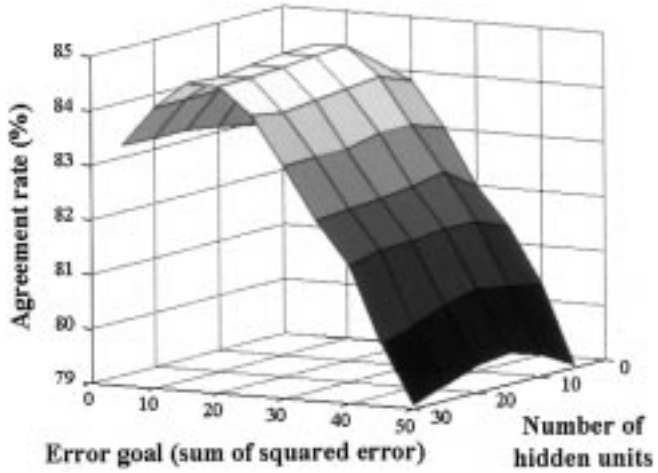

Fig. 5. Averaged performance map according to the error goals and the number of hidden units. The performance of the network could be optimized at the error goal of 20 (sum of squared error). The number of hidden units did not seem to significantly influence the performance of the networks. However, the agreement rate tended to increase as the number of hidden units decreased. Agreement rate was maximal with ten hidden units. The network showed a maximum average agreement rate when it was trained with ten hidden units and an error goal of 20. Maximum average agreement rate was 85%.

TABLE III
OVERALL AGREEMENT RATES WITH THE DIAGNOSIS BY THE HUMAN EXPERTS

Method	Agreement Rate (%)
Artificial Neural Networks	85.0
Linear Discriminant Analysis	69.7
Other Human Expert	80.5

D. Representative Examples of the Performance of the Optimized Network

Figs. 6–9 are the representative examples of the concordant or discordant cases among the test sets diagnosed by a network with the expected performance (agreement rate of 85.0%).

Fig. 6 shows PET images (upper) and the profile of the asymmetry index (lower) in a patient who was classified as NA by both human experts and the network. The dotted line with vertical bars in the lower curves represents the mean and the standard deviations of the NA group of patients. The solid line corresponds to the profile of the asymmetry index of this patient. No area was found with hypometabolism on FDG PET. All the asymmetry indexes of this patient lay within the range of normal mean $\pm(1 \times$ standard deviation$)$ values.

Fig. 7 shows a patient who was classified as left TLE by both the human experts and the network. Human experts diagnosed this case as left TLE on the basis of the slightly decreased metabolism in both the left medial and lateral temporal area shown in the coronal view and in the left anterior temporal lobe shown in the transaxial view. Since the asymmetry of the metabolism was not obvious and the metabolism of the right medial temporal lobe was decreased more than that of the left side (green arrow in coronal view), it was one of the difficult cases for the human experts to diagnose. The metabolic differences in the medial and lateral temporal lobe were also small, in the profile of the asymmetry. The profile of the asymmetry properly represented the asymmetries in the other temporal areas including the anterior temporal lobe. The successful diagnosis by ANN may be based on these findings.

Fig. 8 shows a patient who was classified as right TLE by both human experts and the network. It was also a difficult case for the human expert to diagnose. Focally decreased metabolism

TABLE IV
COMPARISON OF THE DIAGNOSIS BY ARTIFICIAL NEURAL NETWORK TO THAT OF THE HUMAN EXPERTS

Diagnosis by Neural Networks	Diagnosis by Human Experts		
	No abnormal findings	Left temporal lobe epilepsy	Right temporal lobe epilepsy
No abnormal findings	80.5	11.4	14.1
Left temporal lobe epilepsy	10.0	87.1	0.5
Right temporal lobe epilepsy	9.5	1.5	85.4
Total	100 %	100 %	100 %

TABLE V
COMPARISON OF THE DIAGNOSIS BY LINEAR DISCRIMINANT ANALYSIS TO THAT OF THE HUMAN EXPERTS

Diagnosis by Linear Discriminant Analysis	Diagnosis by Human Experts		
	No abnormal findings	Left temporal lobe epilepsy	Right temporal lobe epilepsy
No abnormal findings	14.1	3.3	2.6
Left temporal lobe epilepsy	46.0	80.2	14.5
Right temporal lobe epilepsy	39.9	16.5	82.9
Total	100 %	100 %	100 %

TABLE VI
COMPARISON OF THE DIAGNOSIS BY THE OTHER EXPERT TO THAT OF THE HUMAN EXPERTS

Diagnosis by the Other Human Expert	Diagnosis by Human Experts		
	No abnormal findings	Left temporal lobe epilepsy	Right temporal lobe epilepsy
No abnormal findings	57.8	10.4	8.6
Left temporal lobe epilepsy	20.3	87.9	3.7
Right temporal lobe epilepsy	21.9	1.7	87.7
Total	100 %	100 %	100 %

in the left inferior temporal area shown in coronal view (green arrow) in comparison to the right side confused the human experts. They diagnosed, however, this case as right TLE since the decreased metabolism in right medial temporal lobe (white

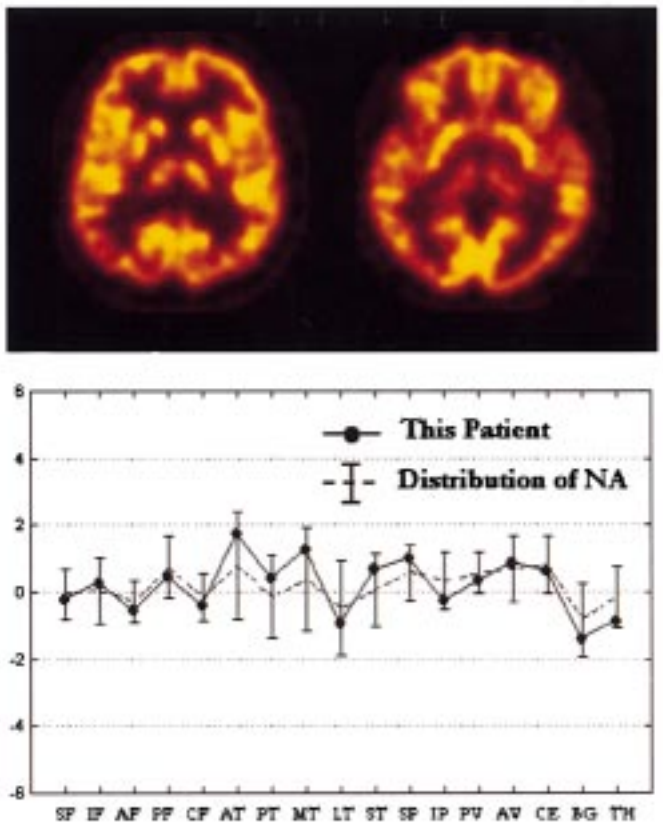

Fig. 6. PET images (upper) and the profile of the asymmetry index (lower) in a patient who was classified as NA by both human experts and the ANN. The dotted line in the lower curves represents the mean and standard deviations of the NA group, and the solid line corresponds to the asymmetry index profile of this patient. No abnormal hypometabolism was shown on PET images. All the asymmetry indexes of this patient described this pattern of PET images and lay within the range of mean $\pm(1 \times$ standard deviation$)$ of the normal distribution.

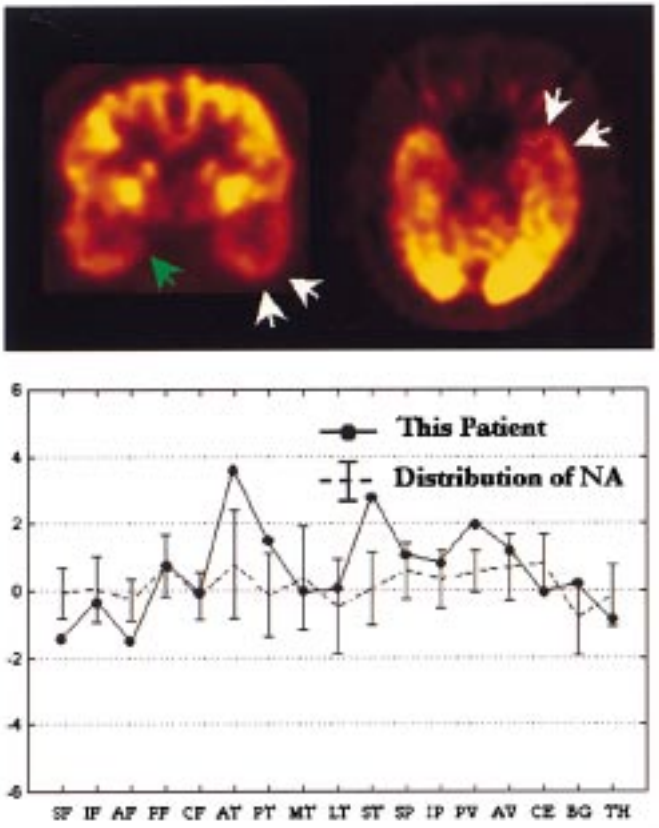

Fig. 7. A patient who was classified as left TLE by both the human experts and the network. Since the asymmetry of the metabolism was not obvious and the metabolism of right medial temporal lobe was decreased more than that of the left side (green arrow in coronal view), it was one of the difficult cases for the human experts to diagnose. The profile of the asymmetry properly represented the asymmetries in the temporal areas including the anterior temporal lobe. The successful diagnosis by ANN may be based on these findings.

arrow in transaxial view) was more apparent. The profile of the asymmetry confirmed that the decreased metabolism in the right medial temporal lobe was more severe than the left side and showed that the metabolism of the right hemisphere was decreased globally.

E. Example of the Case with Erroneous Determination

Fig.9 is the case of a patient who was differently classified by the human experts (left TLE) and most of the networks as well as this one (right TLE). The profile of the asymmetry index represented the decreased metabolism in the right hemisphere. This distribution was obviously shown in the left PET image (white arrows). Human experts, however, diagnosed this patient as left TLE on the basis of the hypometabolism in the left anterior temporal lobe indicated by the green arrow. The profile of the asymmetry index showed that there was no metabolic difference in both the anterior temporal (AT) areas. This seems to be because that the extent of the hypometabolic area was very small compared with that of the AT area, which we defined.

IV. Discussion

In this study, we designed an optimal artificial intelligence classifier for the diagnosis of epileptogenic zones and investigated the performance of this classifier by examining the agreement rates of the diagnosis in comparison to that of human experts. As distribution of regional cerebral glucose metabolism in epilepsy is characteristic on FDG PET, input parameters could be extracted easily from the PET images by referring simply to the pattern of asymmetry. Asymmetric indexes for mirrored regions representing decreased regional cerebral glucose metabolism were used as input parameters to train our ANN.

The optimal range of the error goal for stopping the training of the network and number of hidden units were estimated by repeated randomized experiments, and found to be 20 (sum of squared error) and ten respectively. When networks trained with these error goal and number of hidden units were tested for their performance, agreement rates between ANN and the human experts averaged at 85.0% for the test set (Fig. 5), which was superior to those of linear discriminant analysis (69.7%) and blind classification by the other human expert (80.5%). The agreements of ANN's developed by other investigators were in the range of 80–86% [9] or the areas (AUC) of receiver-operating characteristic (ROC) curves were about 0.9 [7] using Tc-99m-HMPAO perfusion SPECT in the discrimination of Alzheimer disease and vascular dementia from normal aging. An ANN designed on FDG PET performed just as well [5]. Page *et al.* [7] insisted that their network performed $(\mathrm{AUC} = 0.91)$ better than

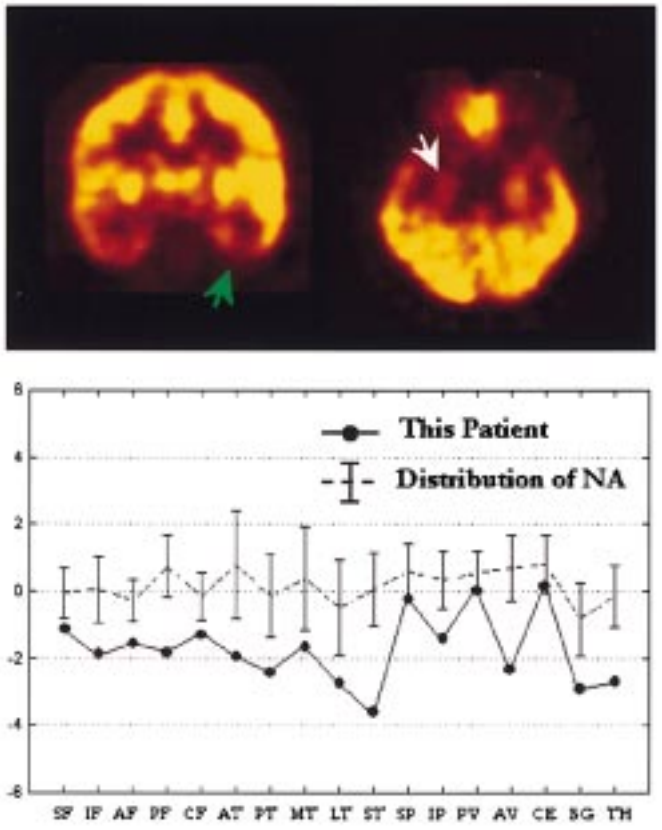

Fig. 8. A patient who was classified as right TLE by both the human experts and the network. Focally decreased metabolism in left inferior temporal area shown in coronal view (green arrow) in comparison to the right side confused the human experts, however, this case was classified as right TLE since the decreased metabolism in right medial temporal lobe (white arrow in transaxial view) was more apparent. The profile of the asymmetry confirmed that the decreased metabolism in the right medial temporal lobe was more severe than the left side, and showed that the metabolism of right hemisphere was decreased globally.

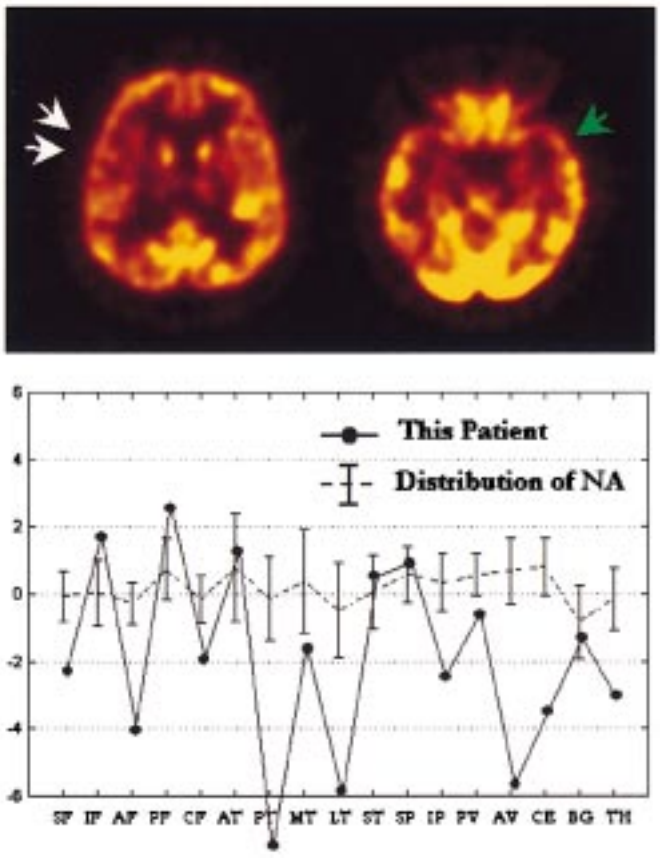

Fig. 9. A patient who was differently classified by the human experts (left TLE) and most networks (right TLE). The profile of the asymmetry index represented the decreased metabolism in right hemisphere. This distribution was obviously shown in left PET image (white arrows). Human expert, however, diagnosed this patient as left TLE on the basis of the hypometabolism in left anterior temporal lobe indicated by gray arrow. The profile of the asymmetry index showed that there was no metabolic difference in both the anterior temporal areas (AT).

that of the alternative statistical techniques $(\mathrm{AUC} = 0.85)$ or even expert viewers $(\mathrm{AUC} = 0.79)$. They had used clinical criteria as a gold standard to examine the performance of their network. In this study we used three sets of images based upon the diagnosis of human experts. Further studies are warranted on the comparative performance of the neural network and human experts, based upon the diagnosis in patients whose epileptogenic zones have been proven by pathology and surgical outcome. After comparing the diagnostic accuracy of the ANN and of human experts, evaluation of the additive value of the ANN would be possible.

Using the ANN developed in this study, we went further to test its performance in localizing other epileptogenic zones in the remaining 60 patients belonging to the other groups. We performed this task to see whether the neural network based its judgment of output diagnosis only on the global asymmetry between the cerebral metabolism of both hemispheres or not. If the network operated in such a manner, we thought that most diagnoses of the other types would all be the left or right TLE. Lateral temporal lobe epilepsy was, however, diagnosed as left or right TLE in 41% of the cases, parietal or occipital lobe epilepsy was diagnosed in 41% of the cases, and frontal lobe epilepsy was diagnosed in 35% of the cases. This result may suggest that our system actually considered hypometabolism in temporal areas as an important factor in its judgment as well as global asymmetry. This may be a good characteristic. Lateralization, moreover, was almost perfect (95%) in these cases.

In this study, we restricted our goal to the classification of temporal lobe epilepsy. This was because the number of subjects in other groups and the amount of resulting data were too small to train the ANN. In order to classify all classes of epilepsy, the adoption of a fuzzy classifier or expert system using prior knowledge provided by human experts would be necessary for our system. We would, of course, also have to recruit more patients belonging to other groups.

We increased the degree of freedom by selecting a multilayered ANN which had the superior ability of self learning without any prior knowledge of diagnostic criteria or decision rules. This multilayered ANN would be able to show that the important property of functional connectivity in the human brain could be represented by complex connections of hidden layers of network. Information about the relationships between specific abnormal cerebral regions and resulting diagnoses could be obtained by analyzing resulting weights between nodes. The ANN developed in this study could be used as a training aid for less experienced physicians, or to highlight the information from FDG

PET for epilepsy experts from different clinical subspecialties as they try to understand FDG PET findings. Further development of integrated diagnostic systems including SPECT, MRI, EEG, and PET is warranted in order to improve the accuracy of localization of epileptogenic zones solely with noninvasive techniques. This ANN could be upgraded to an integrated artificial intelligence system using this approach.

V. Conclusion

We conclude that our ANN performed as well in diagnosing epileptogenic zones on FDG PET as human experts and could be used as a clinical decision support tool for the localization of epileptogenic zones on FDG PET.

References

[1] S. S. Spencer, W. H. Theodore, and S. F. Berkovic, "Clinical applications: MRI, SPECT, and PET," *Magn. Reson. Imaging*, vol. 13, pp. 1119–1124, 1995.

[2] C. R. Jack Jr., B. P. Mullan, F. W. Sharbrough, G. D. Cascino, M. F. Hauser, K. N. Krecke, P. H. Luetmer, M. R. Trenerry, P. C. O'Brien, and J. E. Parisi, "Intractable nonlesional epilepsy of temporal lobe origin: Lateralization by interictal SPECT versus MRI," *Neurology*, vol. 44, pp. 829–836, 1994.

[3] J. J. Frost and H. S. Mayberg, "Epilepsy," in *Principles of Nuclear Medicine.*, H. N. Wagner, Z. Szabo, and J. W. Buchanan, Eds. Philadelphia, PA: W. B. Saunders , 1995, pp. 564–575.

[4] J. M. Links and M. D. Devous Sr., "Detection and comparison of patterns in images," *J. Nucl. Med.*, vol. 35, pp. 16–17, 1994.

[5] J. S. Kippenhan, W. W. Barker, J. Nagel, C. Grady, and R. Duara, "Neural-network classification of normal and Alzheimer's disease subjects using high-resolution and low-resolution PET cameras," *J. Nucl. Med.*, vol. 35, pp. 7–15, 1994.

[6] J. S. Kippenhan, W. W. Barker, S. Pascal, J. Nagel, and R. Duara, "Evaluation of a neural-network classifier for PET scans of normal and Alzheimer's disease subjects," *J. Nucl. Med.*, vol. 33, pp. 1459–1467, 1992.

[7] M. P. Page, R. J. Howard, J. T. O'Brien, M. S. Buxton-Thomas, and A. D. Pickering, "Use of neural networks in brain SPECT to diagnose Alzheimer's disease," *J. Nucl. Med.*, vol. 37, pp. 195–200, 1996.

[8] K. H. Chan, K. A. Johnson, J. A. Becker, A. Satlin, J. Mendelson, B. Garada, and B. L. Holman, "A neural network classifier for cerebral perfusion imaging," *J. Nucl. Med.*, vol. 35, pp. 771–774, 1994.

[9] R. J. deFigueiredo, W. R. Shankle, A. Maccato, M. B. Dick, P. Mundkur, I. Mena, and C. W. Cotman, "Neural-network-based classification of cognitively normal, demented, Alzheimer disease and vascular dementia from single photon emission with computed tomography image data from brain," *Proc. Nat. Acad. Sci. USA*, vol. 92, pp. 5530–5534, 1995.

[10] Z. Szabo, P. F. Kao, W. B. Mathews, H. T. Ravert, J. L. Musachio, U. Scheffel, and R. F. Dannals, "Positron emisson tomography of 5-HT reuptake sites in the human brain with C-11 McN5652 extraction of characteristic image by artificial neural network analysis," *Behav. Brain Res.*, vol. 73, pp. 221–224, 1996.

[11] D. L. Collins, P. Neelin, T. M. Peters, and A. C. Evans, "Automatic 3D intersubject registration of MR volumetric data in standardized Talairach space," *J. Comput. Assist. Tomogr.*, vol. 18, pp. 192–205, 1994.

[12] K. J. Friston, C. D. Frith, P. F. Liddle, and R. S. J. Frackowiak, "Plastic transformation of PET images," *J. Comput. Assist. Tomogr.*, vol. 15, pp. 634–639, 1991.

[13] K. J. Friston, J. Ashburner, C. D. Frith, J.-B. Poline, J. D. Heather, and R. S. J. Frackowiak, "Spatial registration and normalization of images," *Human Brain Mapping*, vol. 3, pp. 165–189, 1995.

[14] J. L. Lancaster, T. G. Glass, B. R. Lankipalli, H. Downs, H. Mayberg, and P. T. Fox, "A modality-independent approach to spatial normalization of tomographic images of the human brain," *Human Brain Mapping*, vol. 3, pp. 209–223, 1995.

[15] C. Davatzikos and R. N. Bryan, "Using a deformable surface model to obtain a shape representation of the cortex," *IEEE Trans. Med. Imag.*, vol. 15, pp. 785–795, Dec., 1996.

[16] P. Tompson and A. W. Toga, "A surface-based technique for warping three-dimensional images of the brain," *IEEE Trans. Med. Imag.*, vol. 15, pp. 402–417, Aug., 1996.

[17] D. E. Rumelhart, G. E. Hinton, and R. J. Williams, "Learning representations by back-propagating error," *Nature*, vol. 323, pp. 533–536, 1986.

[18] L. Fausett, "Backpropagation Neural Net," in *Fundamentals of Neural Networks: Architectures, Algorithms, and Application*. Englewood Cliffs, NJ: Prentice-Hall, 1994, pp. 289–330.